Advanced Steel Construction – Vol. 20 No. 2 (2024) 199–207
DOI: 10.18057/IJASC.2024.20.2.12
(Special Issue: *11st International Conference on Advances in Steel Structures, ICASS'2023, Kuching, Sarawak, Malaysia*)

FLEXURAL BEHAVIOR OF REINFORCED HOLLOW HIGH STRENGTH CONCRETE FILLED SQUARE STEEL TUBE

Zhi-Jian Yang *, Shu Zhang, Wei-Zhe Cui and Guo-Chang Li

School of Civil Engineering, Shenyang Jianzhu University, Shenyang, PR China
** (Corresponding author: E-mail: faemail@163.com)*

ABSTRACT

Flexural behavior of reinforced hollow high strength concrete filled square steel tube was studied through test and finite element analysis. Six specimens were designed to consider effects of steel ratio and reinforcement ratio. The failure modes, bending moment-curvature curve, load-strain curve and distribution of the deflection curves were analyzed. The results showed that the steel tube, PHC column, sandwich concrete can work well together subjected to bending moment. The change process of moment-curvature curve of specimen could be divided into three stages: elastic stage, elastic-plastic stage and hardening stage. The ultimate bearing capacity of the member increases with the increase of thickness of steel tube. The ultimate bearing capacity of member reinforced with deformed bars is higher than that of non-reinforcement. In addition, the three-dimensional finite element model was established by using ABAQUS software to analyze the behavior of members. Based on the experimental and numerical results, the simplified formula for calculating the flexural capacity of members was proposed. The calculated results are consistent well with the experimental results.

ARTICLE HISTORY

Received: 8 April 2024
Revised: 20 April 2024
Accepted: 5 June 2024

KEYWORDS

Reinforced hollow concrete filled square steel tube;
High strength concrete;
Flexural behavior;
Load sharing

1. Introduction

Concrete filled steel tube (CFST) is composed of filled concrete and steel tube with the advantages of high bearing capacity, good ductility and fire resistance, which is widely used in high-rise building, long-span bridges [1, 2]. In actual engineering, concrete-filled steel tube columns will bear bending moment under wind load and horizontal earthquake [3, 4], so it is necessary to study their flexural performance.

A lot of research about the flexural behavior of CFST members had been done in recent years. Elchalakani et al [5] presented the experimental results of the flexural behavior of circular concrete filled tubes under pure bending, which showed that the filled concrete enhances strength, ductility and energy absorption especially for thinner sections. Han et al [6, 7] conducted pure pending tests on 36 specimens, and four kinds of different parameters were considered, and the calculation formulae of moment versus curvature curves and the flexural stiffness were presented. Elchalakani and Zhao [8] investigated the cyclic flexural behavior of concrete-filled cold-formed circular steel tubes. Moon et al [9] used numerical models to predict the confinement effects, composite action, and flexural behavior of concrete-filled steel tubes, and proposed a simplified model. Wang et al [10] presented a FEA modeling to study the flexural behavior of rectangular concrete filled steel tubular members with compact, non-compact or slender element sections. Zhan et al [11] proposed prestressed concrete-filled steel tube to increase its enhancement as subjected to flexure. Javed et al [12] carried out numerical investigations to study the flexural behavior of square and rectangular steel tubes filled with normal and high strength concrete. Chen et al [13] reported the pure bending test results of 28 circular concrete-filled aluminum alloy tubes, which demonstrated that the large wall thickness of aluminum alloy tube improved the bearing capacity, the bending deformation capacity and the ductility of specimens. AL-Shaar and Gogus et al [14] reported the test results of flexural behavior of lightweight concrete and self-compacting concrete filled square steel tube beams. Liu et al [15] investigated the failure mechanism of concrete-filled steel circular tube support, and proposed welding steel at the vault and the spring line to improve flexural bearing capacity. Al Zand et al [16] conducted experimental and numerical investigations on the flexural performance of concrete-filled square steel tube stiffened with V-shaped grooves. Li et al [17] reported the test and numerical analysis results of high-strength concrete filled high-strength square steel tubes subjected cyclic pure bending, which indicated that the members had excellent energy dissipation capacity and ductility. Li et al [18] investigated the flexural performance of UHPC filled high-strength steel tube and UHPC filled double skin high-strength steel tube, which indicated that the composite action between UHPC and high-strength steel tube was efficient. Wang et al [19] investigated the flexural behavior of high-strength rectangular concrete-filled steel tube members by test and FEM, which indicated that the members with high-strength steel tubes had lower ductility compared with conventional-strength CFST member.

Hollow concrete filled steel tube (HCFST) is an important form of CFST, many researches have been conducted to study its behavior [20, 21, 22, 23, 24]. The bearing capacity, ductility and seismic performance of HCFST columns are lower than solid CFST columns. Therefore, the application scope of HCFST is limited, which is usually used in power transmission tower. To improve the behavior of HCFST, the reinforced hollow concrete filled steel tube (RHCFST) was proposed by Yang et al [25], which is composed by steel tube, PHC column and sandwich concrete. The flexural behavior of RHCFST members was studied by experiment, finite element analysis and theoretical analysis. A general method for calculating the flexural bearing capacity of members is proposed.

2. Experimental investigation

2.1. Specimen design

Six reinforced hollow high-strength concrete-filled square steel tube beams with varying parameters like steel tube thickness and deformed steel bars were designed. The cross section of the specimen is 400mm×400mm, and its length is 2800mm, as shown in Fig. 1. Q235 steel was used to make the tube. C80 and C60 are the compressive strengths of prestressed high strength concrete (PHC) column concrete and sandwich concrete, respectively. Table 1 shows the detailed parameters of the specimens.

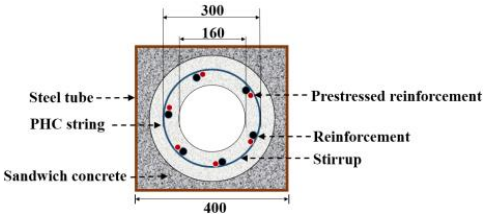

Fig. 1 Cross section of specimen

Table 1
Specimen parameters

Specimen	*t*/mm	Prestressed bars	Deformed steel bars	L_0/mm	ξ
BRHCFST-1	5	6A7.1	6B16	2400	0.234
BRHCFST-2	5	6A7.1	--	2400	0.234
BRHCFST-3	6	6A7.1	6B16	2400	0.284
BRHCFST-4	6	6A7.1	--	2400	0.284
BRHCFST-5	8	6A7.1	6B16	2400	0.386
BRHCFST-6	8	6A7.1	--	2400	0.386

2.2. Material properties

The properties of steel were determined in accordance with Metallic Materials-Tensile testing-Part 1: Method of test at room temperature (GB/T288.2010), which are detailed in Table 2. Commercial concrete was used to create sandwich concrete. The PHC column was prefabricated in factory. The concrete strength was determined using the GB/T 50081-2019 Standard for Test Methods of Concrete Physical and Mechanical Properties. The compressive strength was tested using three 150mm×150mm×150mm cubic standard test blocks. The cubic compressive strengths of PHC columns and sandwich concrete are 77.7MPa and 71.3MPa, respectively.

Table 2
Properties of the bars and steel tube

	t/mm	d/mm	f_y/MPa	f_u/MPa	E_s/GPa
Prestressed bar	-	7.1	1465	1536	208.2
Deformed bar	-	16	459	650	199.5
Stirrup	-	4	631	692	215.5
Steel tube	5	-	358	503	189.7
	6	-	454	493	172.7
	8	-	363	484	190.7

Note: t is the thickness of steel tube, d is the diameter of reinforcement, fy is the yield strength, fu is tensile strength, and Es is elastic modulus

2.3. Test setup

The load was applied by the NYL-5007T testing machine with three-point loading method, as shown in Fig. 2. The deflection was recorded using three displacement transducers. As shown in Fig. 2(b), two displacement transducers (W-4 and W-5) were placed at the positions of the supports to measure their displacement. As shown in Fig. 2(c), twenty-four strain gauges were pasted on the steel tube to record the change in strain. The grading loading system was used in the test, and the load of each stage is about 1/15 of the ultimate bearing capacity, with each load lasting 2 minutes..

(a) Photo of loading device

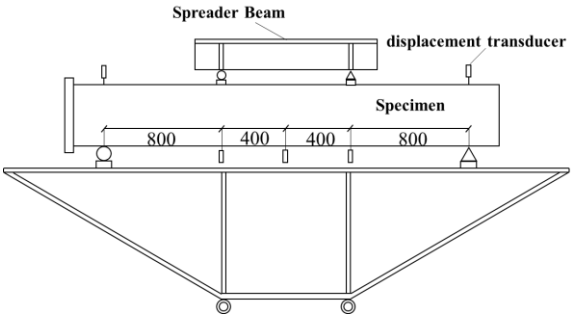

(b) Diagrammatic view

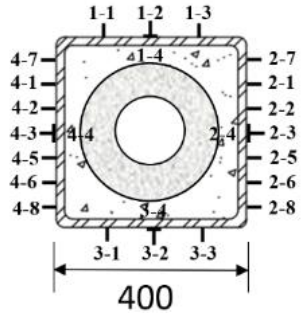

(c) Location of strain gauges

Fig. 2 Layout of loading device

2.4. Test results and discussions

2.4.1. Test phenomenon

At the beginning of the test, the load-deflection curve of specimen BRHCFST-1 grew linearly, suggesting that the specimen was in the elastic stage and had undergone no noticeable deformation. When the load reached 270.1kN, the specimen made a small noise and the concrete in the tension zone fractured. When loaded to 810.2kN, the steel tube in the tension zone reached yield strength. As the load grew, the transverse deformation of the concrete started to exceed that of the steel tube, and the confinement effect could be seen in the local buckling that started to occur in the compression zone of the steel tube's mid-span section. The specimen had reached the stage of elastic-plasticity. When loaded to 1348kN, the concrete made a continual cracking sound. When the load is greater than the specimen's ultimate bearing capacity of 1352.2kN, the load-deflection curve exhibits a decreasing trend. Fig. 3 depicts the overall failure mode and local buckling of BRHCFST-1 at the middle span.

(a) Over all failure mode

(b) Local buckling

Fig. 3 Failure mode of specimen BRHCFST-1

2.4.2. Failure mode

As loaded to 0.7P, the specimens began to appear obvious bending deformation gradually, and the deflection in the mid-span increased rapidly. When loaded to the ultimate bearing capacity, the steel tube on the compression surface appeared local buckling, as shown in Fig. 3(b). The test was terminated when the deflection reached L/50. After the mid-span deflection reached 48mm (L_0/50), the flexural bearing capacity of the specimen was still increasing, which indicates that the specimen has good ductility.

To further investigate the crack development and failure of the concrete of the typical specimen, the steel tube of the specimen BRHCFST-5 was removed, as shown in Fig. 4. The sandwich concrete was crushed at the position of steel tube buckling, the buckling near the loading point is obvious. There are several cracks in the tension zone of the pure bending section of the specimen, extending from the tension zone to the compression zone, about 3/4 of the height. The crack width of the core concrete is about 1~2mm, which is uniformly distributed, and the largest crack is about 5mm near the mid-span section. It could be found that reinforcement has obvious confinement effect on crack propagation of concrete. The larger the reinforcement ratio is, the slower the crack propagation is.

(a) Tensile side of sandwich concrete

(b) Compression side of sandwich concrete

(c) Side face of core concrete

(d) Tensile side of core concrete

Fig. 4 Failure mode of concrete

2.4.3. Distribution of the deflection curves

Fig. 5 shows the deflection distribution curves of specimens along the length. The solid line depicts the deflection curves of specimens subjected to various loads, the abscissa L represents the distance from the left end hinge, and the ordinate represents the deflection value. As shown in Fig. 5, the deflection of each measurement point increases as the load grade increases, and the shape of the deflection curve of the specimen under each load level is essentially a sinusoidal half-wave curve. Throughout the whole loading phase, the specimen deformation is essentially symmetrical and in good accord with the standard sine half-wave curve.

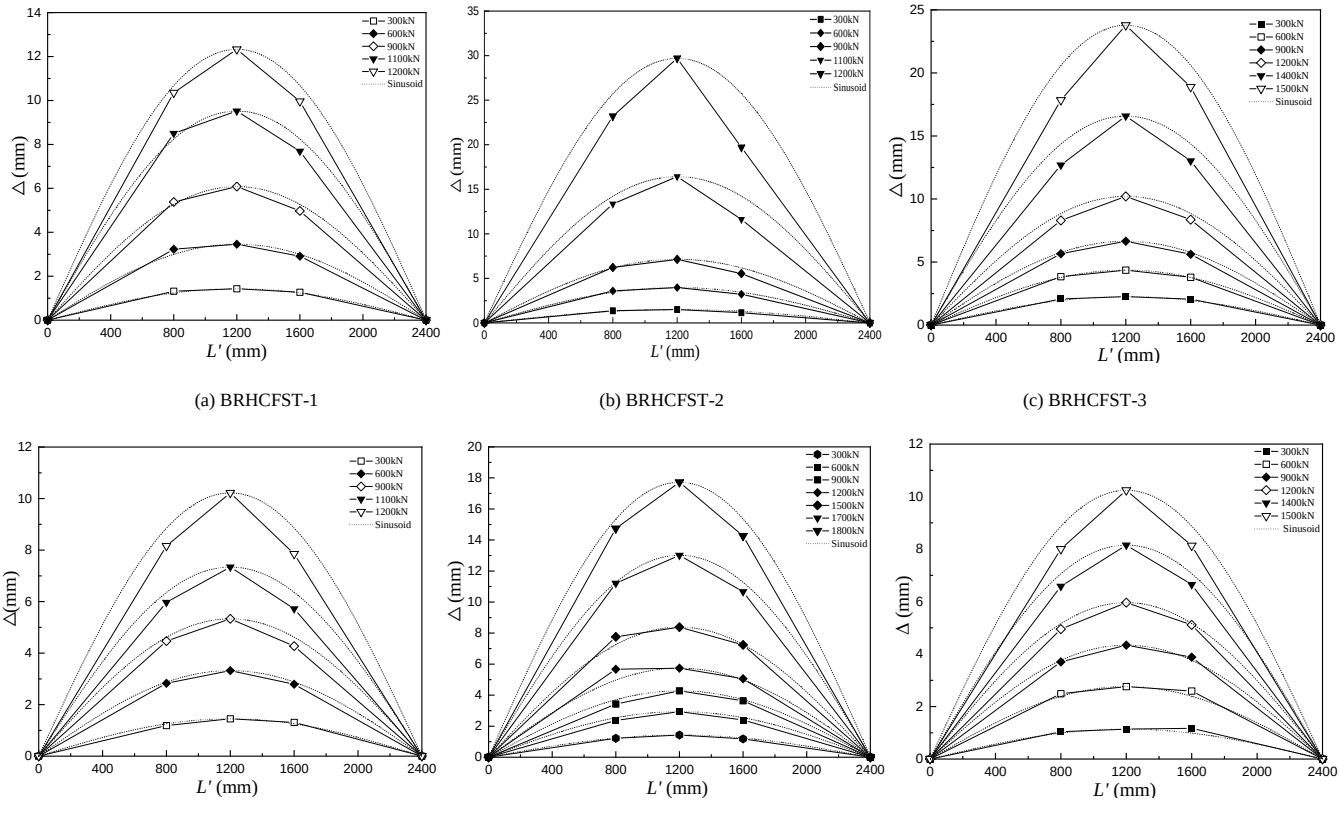

(a) BRHCFST-1 (b) BRHCFST-2 (c) BRHCFST-3

(d) BRHCFST-4 (e) BRHCFST-5 (f) BRHCFST-6

Fig. 5 Distribution of the deflection curves.

2.4.4. Load-strain curves

The specimen load-strain curves are shown in Fig. 6. In the first stage of loading, the longitudinal strain of the compression zone and the tension zone of the steel tube are comparable, and the strain grows essentially linearly. Because the concrete in the compression zone and the steel tube together support the load, when the concrete in the tension zone fractures, the rate of strain change in the tension zone is greater than in the compression zone. The steel tube in the tension zone initially reaches the elastic-plastic stage as the load increases, and the strain growth rate accelerates. After the steel tube in the compression zone has yielded, it enters the elastic-plastic stage and the entire portion of the specimen begins to deform plastically.

2.4.5. Longitudinal strain distribution

The longitudinal strain curves of the specimens at various load levels along the height of the mid-span section are shown in Fig. 7. F is the specimen's ultimate bearing capacity when the tension strain of the steel tube reaches 10000. As seen in Fig. 7, the strain connection is roughly a straight line during the whole loading procedure. Therefore, the deformation of the pure bending section conforms to the assumption of the plane section. The neutral axis is located at the junction of the strain distribution curve and the point X=0 under different loads. Prior to applying load, the neutral axis of the specimen's mid-span section coincides with the section's centroidal axis. When the load reaches 0.2F, the height of the neutral axis moves 0.08~0.1h higher than that of the centroidal axis, and the neutral axis rises at a quicker rate. As the load increases, the neutral axis begins to migrate much higher within the compression zone. When the load reaches about 0.6F, the neutral axis rises about 0.11~0.18h, but the rate of ascent slows. With the continuous increase of load, the rising speed of neutral axis tends to be stable. As the load continues to increase, the rising speed of the neutral axis tends to remain stable. When the load exceeds F, the neutral axis increases between 0.25 and 0.31h.

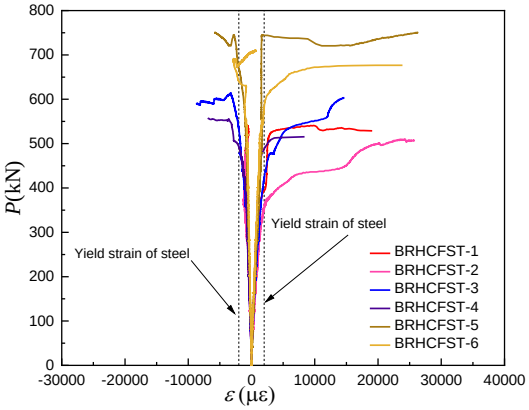

Fig. 6 Load - strain curves of specimens

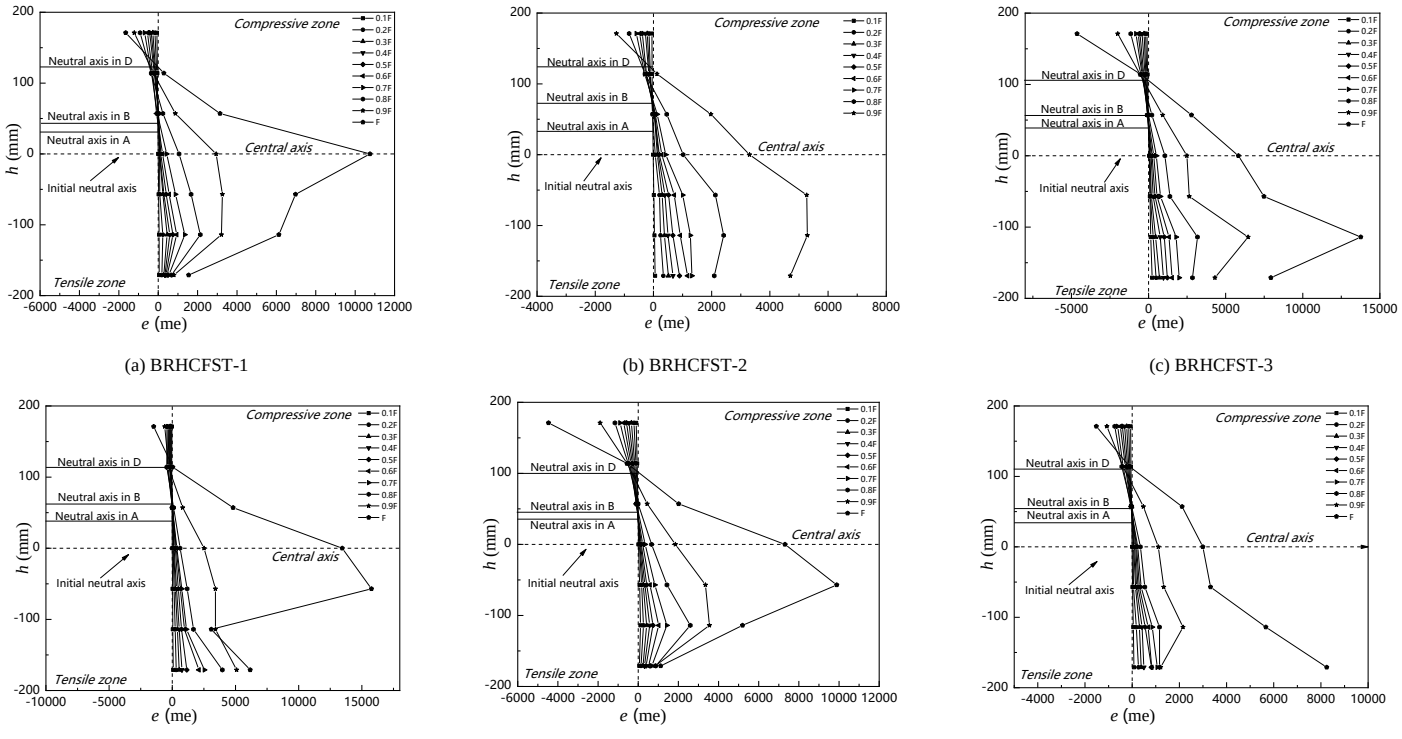

(a) BRHCFST-1 (b) BRHCFST-2 (c) BRHCFST-3

(d) BRHCFST-4 (e) BRHCFST-5 (f) BRHCFST-6

Fig. 7 Longitudinal strain distribution at mid-span

2.4.6. Bending moment-curvature curves

The curvature of the specimen can be calculated by Equ (1). Where Δ_m is the deflection of middle-span, x is the distance from the mid-span section to the support, and l0 is the effective span of the specimen.

$$\phi = (\pi^2 / l_0^2)\Delta_m \sin(\pi x / l_0) \quad (1)$$

Fig. 8 illustrates the moment-curvature curve of the specimen. When the bending moment reaches point A (M_A=0.2M_{ue}), the stiffness changes slightly, the concrete in the tensile zone of the specimen occurs cracks, and the bending stiffness decreases slightly. At point B (M_B=0.6M_{ue}), the tension zone of steel tube yields. At point C (M_C=0.8M_{ue}), compression zone of the steel tube yields. The specimen reaches the ultimate bending moment at Point D (M_D=M_{ue}) is the ultimate bearing capacity. After exceeding the ultimate bearing capacity, the bearing capacity of the member is continuing increasing, but the deformation is too large, so it is unloaded at point E and the test is ended.

Fig. 8 shows that moment-curvature curves can be divided into three stages: elastic stage, elastic-plastic stage and hardening stage. The behavior of each stage is as follows:

Elastic stage (OB): There is no visible change in the specimen during the initial stage of loading. Steel tube and concrete are both in the elastic stage, and their interaction is minimal. The concrete is compressed biaxially in the compression zone, while the transverse deformation of the steel tube is constrained. Bending moment growth is obviously faster than curvature growth, specimen flexural deformation is smaller, and the neutral axis rises slowly. The specimen reaches the proportional limit when the bending moment reaches M_A=0.2M_{ue}, and the concrete in the tension zone cracks when it reaches the ultimate tensile strain of concrete. As a result, the tensile strength of concrete has little effect on the overall mechanical behavior of specimens. Only the effect of tensile stress on steel tube is considered in the tension area, while the effect of concrete is ignored.

Elastic-plastic stage (BD): The maximum tensile stress of steel tube reaches

the yield strength when the bending moment reaches M_B=0.6M_{ue}. The longitudinal compressive stress of concrete continues to rise, and because steel tube has a lower transverse deformation coefficient than concrete, the hoop stress caused by deformation between steel tube and concrete rises as well. The stress in the steel tube greatly exceeds the proportional limit in the tension zone until the steel tube yields. When the bending moment reaches M_C=0.8M_{ue}, the yield strength of the steel tube in the compression zone is reached. The neutral axis rises obviously, but at a slower rate than in the elastic stage, and the rate of curvature growth is faster than the rate of bending moment.

Hardening stage (DE): The specimen enters the hardening stage when the ultimate bending moment M_D=M_{ue} is reached. The hoop stress between steel tube and concrete increases as transverse deformation increases. The bending moment of the specimen does not show a downward trend, the deflection of the specimen increases, and the specimen has undergone obvious large deformation. The specimens exhibit good ductility without brittle fracture due to the good cooperation between steel tube and concrete. Bending moment increases at a slower rate than curvature.

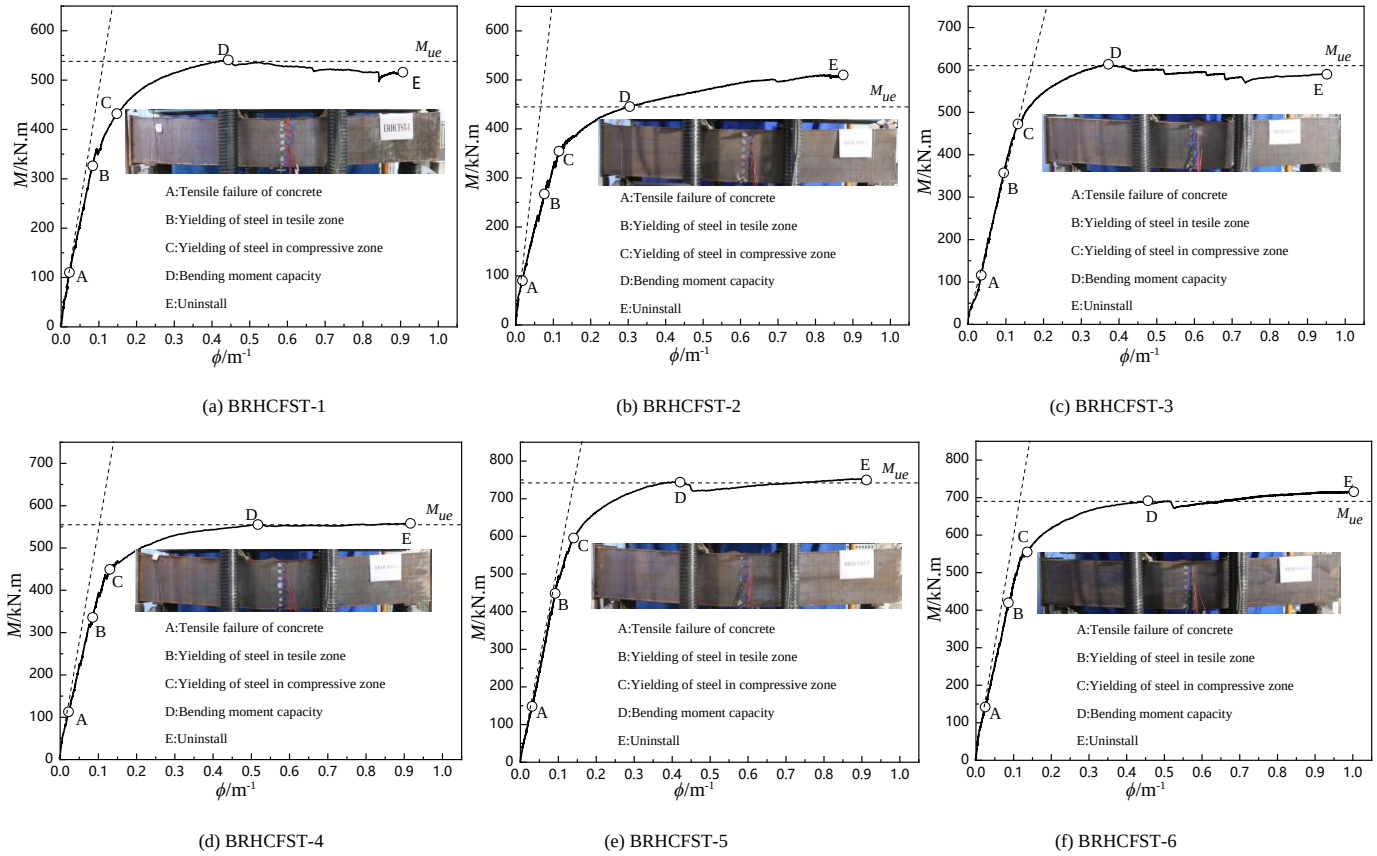

(a) BRHCFST-1 (b) BRHCFST-2 (c) BRHCFST-3

(d) BRHCFST-4 (e) BRHCFST-5 (f) BRHCFST-6

Fig. 8 Bending moment-curvature curves

3. Finite element analysis

3.1. Material constitutive model

3.1.1. Steel

Steel tube stress-strain relationship curve used the five fold line model, and the modulus of strengthening section is 0.01E_s. The bilinear model was used for deformed bars, prestressed bars, and spiral stirrups.

3.1.2. Concrete

The PHC column concrete used the compressive stress-strain relationship of concrete proposed by Guo [26] The modified simplified model considering confinement effect coefficient was adopted in the constitutive model of sandwich concrete [27]. Prestress of PHC column was applied by decreasing temperature method.

3.2. Model establishment

The steel tube, concrete and the endplate adopted a three-dimensional solid element (C3D8R) with 8-node reduction integral format. Surface-to-surface contact was used for the interaction between steel tube and concrete, the normal direction of the interface used hard contact, the tangential direction of the interface used the Coulomb friction model, and the friction coefficient was 0.6 [28]. Hard contact was adopted between endplate and concrete, tie contact was used between steel tube and endplate, and surface-to-surface contact was adopted between sandwich concrete and PHC column concrete. As shown in Fig. 9, the reference points were established at the third point on the upper surface of the specimen, and the displacement-controlled loading method was used to model the pure bending members.

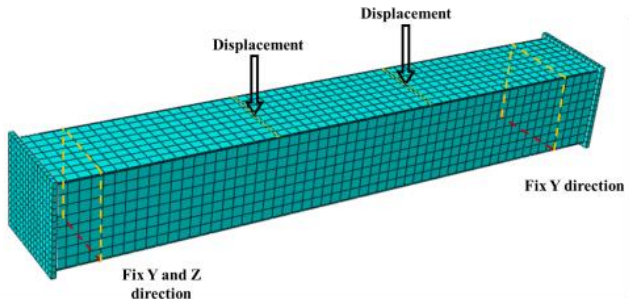

Fig. 9 Simulation boundary conditions.

3.3. Comparison between FEA and test results

Fig. 10 shows a comparison of the failure mode between finite element analysis and the test of specimen BRHCFST-1. The failure modes of the two are quite consistent, as shown in Fig. 10. The results of the finite element analysis are compared to the experimental moment-deflection curve shown in Fig. 11. The FEA results are in good agreement with the experimental bending moment and bending stiffness, as shown in Fig. 11. Table 3 shows that the maximum difference in bending moment is 8.06%. The findings demonstrate that the finite element model accurately simulates and analyzes the flexural behavior of a reinforced hollow high concrete filled square steel tube.

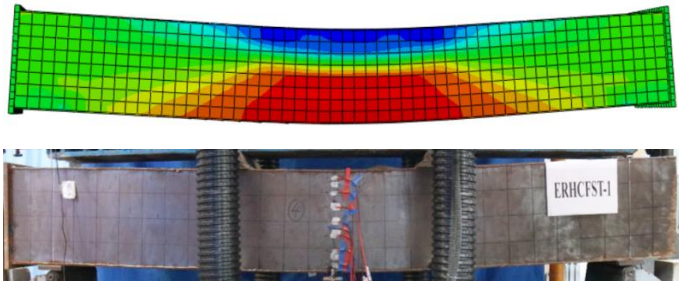

Fig. 10 Comparison of the failure mode

Table 3
Comparison of the ultimate bearing capacity and deflection

Specimen	FEA		TEST		M_s/M_u	Δ_s/Δ_u
	M_s(kN· m)	Δ_s(mm)	M_u(kN· m)	Δ_u(mm)		
BRHCFST-1	533.5	28.0	540.9	25.9	0.99	1.1
BRHCFST-2	484.0	26.0	445.0	17.7	1.08	1.5
BRHCFST-3	605.4	26.5	614.0	21.7	0.99	1.2
BRHCFST-4	550.9	31.5	556.0	30.6	0.99	1.0
BRHCFST-5	739.5	27.0	744.0	24.4	0.99	1.1
BRHCFST-6	678.9	31.8	691.5	26.6	0.98	1.2

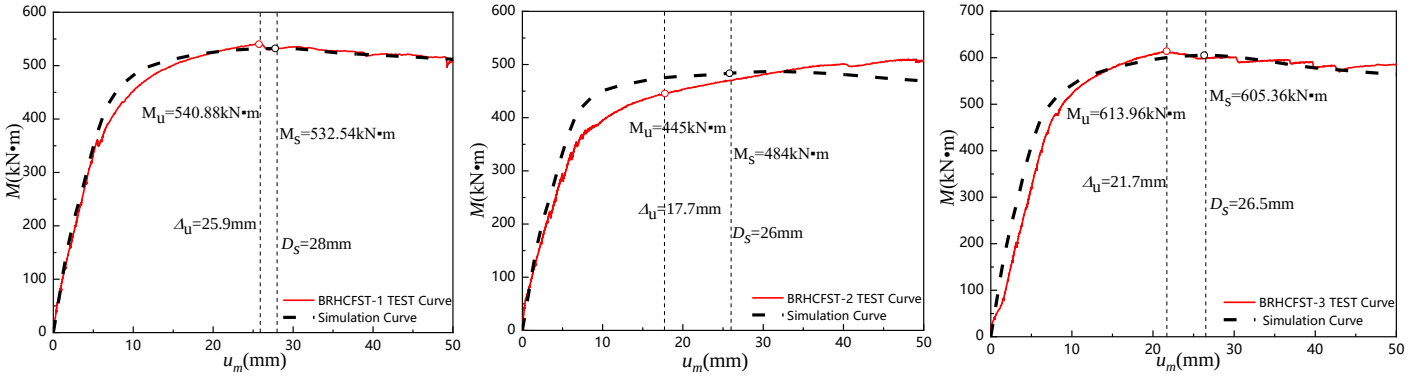

(a) BRHCFST-1 (b) BRHCFST-2 (c) BRHCFST-3

(d) BRHCFST-4 (e) BRHCFST-5 (f) BRHCFST-6

Fig. 11 Comparison of moment-deflection between simulation and test results.

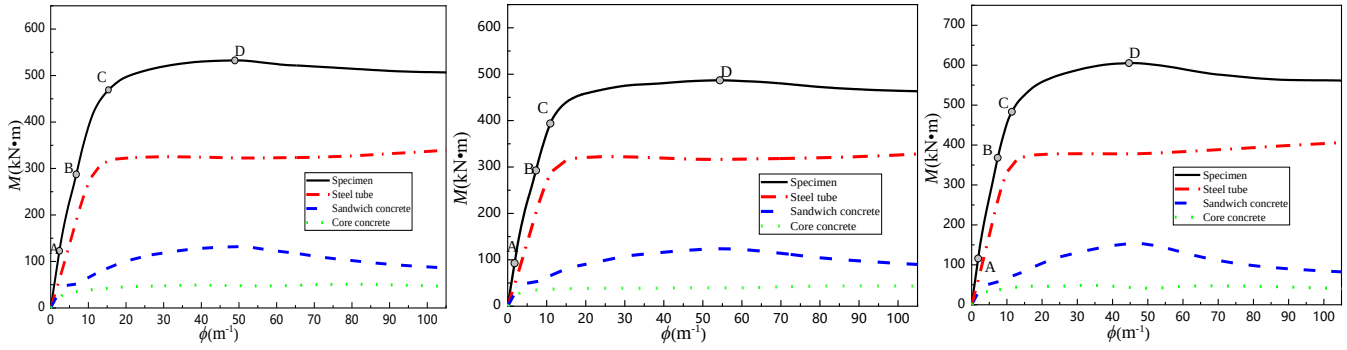

(a) BRHCFST-1 (b) BRHCFST-2 (c) BRHCFST-3

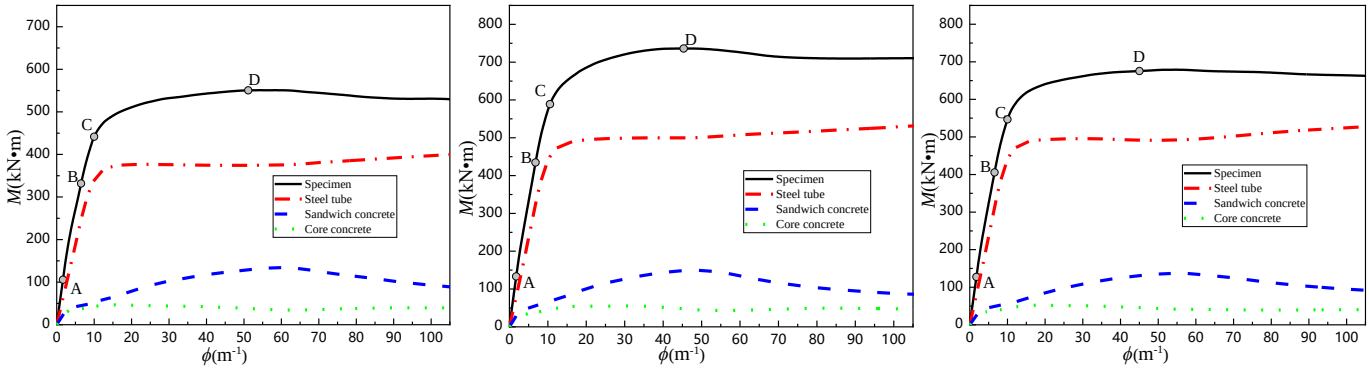

(d) BRHCFST-4 (e) BRHCFST-5 (f) BRHCFST-6

Fig. 16 The moment-deflection curve of each component

3.4. Load sharing of each component

Fig.16 show the bending moments of steel tube, sandwich concrete and PHC column concrete throughout the loading process. Before point A, the steel tube bears more than half of the bending moment, which is about 48.9%~63%, because at the initial stage of loading, the steel tube shares most of the load. The steel tube reaches the peak point after point C, and the bending moment is 67%~80%, and then decreases slowly. The bending moment of sandwich concrete at point D accounts for 19.4%~24.9% of the total bending moment. At this time, it reaches the peak point and then decreases. After the peak point, the curve of PHC column concrete tends to be smooth. Fig. 16 and Table 6 show that the load sharing ratio of steel tube decreases with the increase of deformed bar ratio and increases with the increase of thickness of steel tube.

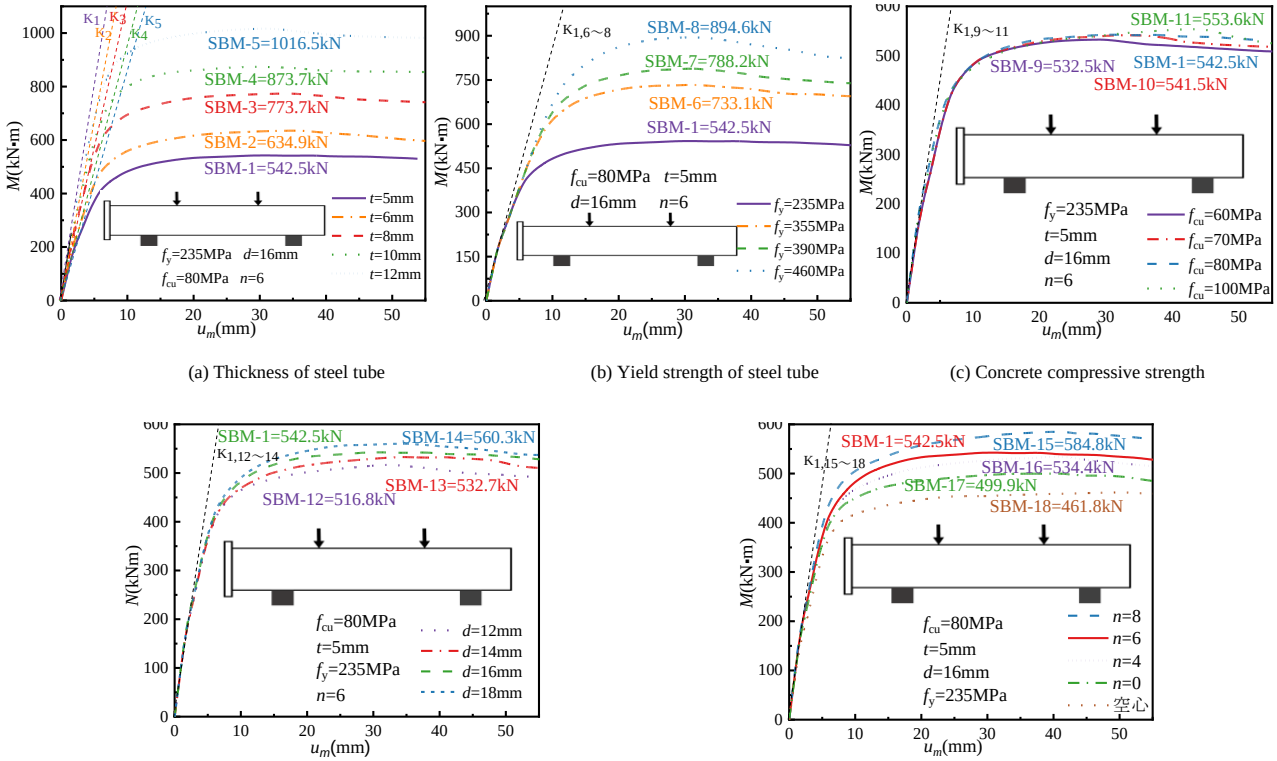

(a) Thickness of steel tube (b) Yield strength of steel tube (c) Concrete compressive strength

(d) Diameter of deformed bars (e) Number of deformed bars

Fig. 17 Moment-deflection curve of different parameters

4. Parameters analysis

To further analyze the influence of different parameters, the steel ratio, steel yield strength, compressive strength of sandwich concrete, the diameter of deformed bars, and number of deformed bars are taken as variables. The design parameters and corresponding results are shown in Fig. 17

4.1. Steel ratio

Fig. 17 (a) shows the moment-deflection curves of members with different steel ratio. The steel tube thickness of model SBM-1, 2, 3, 4 and 5 are 5, 6, 8, 10 and 12mm, respectively. The ultimate bending moments of model SBM-2, 3, 4 and 5 are 113.7%, 138.9%, 160.4% and 185.9% of SBM-1 respectively. The confinement coefficient increases with the increase of steel ratio. The change of steel ratio has a certain influence on the initial stiffness. At the initial stage of loading, the steel tube bears most of the bending moment, at this time, the role of concrete and reinforcement is relatively small, so changing the steel ratio has a great influence on the initial stiffness.

4.2. Steel yield strength

Fig. 17 (b) shows the moment-deflection curves of members with different steel yield strength. The yield strength of model SBM-1, 6, 7 and 8 is 235MPa, 345MPa, 390MPa and 550MPa, respectively. The ultimate bending moments of models SBM-6, 7 and 8 are 132%, 143.8% and 161.6% of SBM-1 respectively. The stiffness of the specimens with different steel strength is the same in the elastic stage. It can be seen from the bending moment distribution that the contribution of steel tube is greater, so when the yield strength of steel is

changed, the bearing capacity changes greatly. Changing the yield strength of steel has no effect on the initial stiffness.

4.3. Concrete compressive strength

Fig. 17 (c) shows the moment-deflection curves of members with different concrete compressive strength. The compressive strength of concrete of model SBM-1, 9, 10 and 11 is 60MPa, 70MPa, 80MPa and 100MPa respectively. The ultimate bending moments of models SBM-9, 10 and 11 are 101.7%, 102.7% and 103.8% of SBM-1, respectively. The change of the compressive strength of concrete has little influence on the bending moment, as shown in Fig. 17. Changing the compressive strength of concrete has no effect on the initial stiffness.

4.4. Diameter of deformed bars

Fig. 17 (d) shows the moment-deflection curves of members with different diameters of deformed bars. The steel diameters of model SBM-1, 12, 13 and 14 are 16mm, 14mm, 12mm and 10mm respectively. The ultimate bending moments of models SBM-12, 13 and 14 are 98.8%, 96.7% and 95.3% of SBM-1 respectively. The diameter of deformed bars has little effect on the ultimate bending moment of the members, and changing the diameter of deformed bars has no effect on the initial stiffness.

4.5. Diameter of deformed bars

Fig. 17 (e) shows the moment-deflection curves of members with different number of deformed bar. The number of deformed bar of model SBM-1, 15, 16 and 17 is 6, 4, 8 and 10 respectively. When the number of deformed bar is changing from 6 to 8, the bearing capacity of the members increases in turn. The member with 8 deformed bars has the highest bearing capacity, which shows a downward trend when it reaches the peak point, and develops steadily, showing good ductility. However, when the number of deformed bars is 10, the bearing capacity of the specimen decreases. The ultimate moment of model SBM-15, 16 and 17 is 97.1%, 105.7% and 103.7% of model SBM-1 respectively. Changing the number of deformed bars has little effect on the initial stiffness. It is recommended that the number of deformed bars to be arranged in the range of 6-8.

5. Calculation formula of flexural bearing capacity

The reinforced hollow high concrete filled square steel tube pure bending member can be regarded as the combination of hollow high concrete filled square steel tube and PHC column, and the two parts are superimposed. The calculation formula of bending bearing capacity is as follows:

$$M = M_{\mathrm{u}} + k_{\mathrm{d}} M_{\mathrm{p}} \tag{2}$$

$$M_u = \gamma_m W_{sc} f_{sc} \tag{3}$$

$$\gamma_m = (1-0.5\psi)(2.379\xi + 0.1819\sqrt{\xi}) \tag{4}$$

$$W_{sc} = \frac{\pi(r_0^{\,4} - r_{ci}^{\,4})}{4r_0} \tag{5}$$

$$f_{sc} = (1.212 + B\xi + C\xi^2) f_c \tag{6}$$

$$\xi = \frac{\mathrm{A_s} \cdot f}{\mathrm{A_c} \cdot f_c} \tag{7}$$

$$\begin{aligned} M_p = {} & (\alpha_1 f_{p\times k} A_{pc} (r_{pi} + r_{p0}) \frac{\sin \pi\alpha}{2\pi} + f_{pi}^{'} A_{pi} r_p \frac{\sin \pi\alpha}{\pi} \\ & + (f_{pit} - \sigma_{po}) A_{pi} r_p \frac{\sin \pi\alpha_1}{\pi} + f_{zi} A_{zz} r_z \frac{\sin \pi\alpha + \sin \pi\alpha_r}{2\pi}) \end{aligned} \tag{8}$$

$$\alpha = \frac{0.55\sigma_{po} + 0.45 f_{ptk} A_{py} + 0.5 f_{sy} A_{ss}}{\alpha_1 f_{pck} A_{pc} + f_{py}^{'} A_{py} + 0.45(f_{ptk} - \sigma_{po}) A_{py} + f_{sy} A_{ss}} \tag{9}$$

Where, M_{u} and M_{p} are the bending bearing capacity of hollow high concrete filled square steel tube and PHC column, respectively. γ_{m} is flexural strength index, W_{sc} is the section modulus of the composite section, f_{sc} is the nominal yield strength of the composite section, ψ is the hollow ratio, ξ is the confinement coefficient, r0 is the equivalent radius, r_{ci} is the hollow radius, f_y is the standard value of concrete compressive strength, B=0.039f/213+0.247, C=-0.006f_c/14.4+0.002, f is the standard value of compressive strength of steel. The symbols in Equ (7) can be found in reference [29].

The average value and standard deviation of the ratio between the calculated results of the bending capacity calculation formula and the simulated value of the finite element are 0.971 and 0.0016

The average value of the ratio of the calculated value of the bending bearing capacity formula to the finite element simulation value is 0.971, and the mean square deviation is 0.0016. Fig. 18 shows the comparison between the finite element analysis results and the bearing capacity calculation formula, and the error is less than 10%. The calculation formula is as follows:

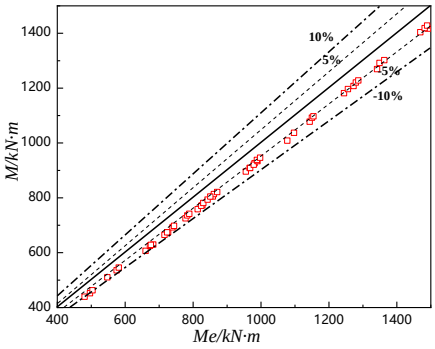

Fig. 18 Comparison of calculated and simulated values.

6. Conclusions

Through the analysis and discussion of the test results and finite element analysis results, the following conclusions can be drawn:

(1) The test results showed that the steel ratio and reinforcement ratio have important effects on the ultimate bearing capacity and ductility. The deflection curve was similar to the standard sinusoidal half wave curve, and the specimen appeared local buckling at the mid-span.

(2) Based on the reasonable constitutive model, a finite element model for simulating the mechanical behavior of reinforced hollow concrete filled square steel tubular beams was established. The finite element calculation results were in good agreement with the experimental results.

(3) In the whole process of stress, the steel tube resists most of the bending moment from beginning to end. The bending moment resistance of sandwich concrete is higher than that of tube column concrete. The pure bending specimen can be divided into elastic stage, elastic-plastic stage and hardening stage.

(4) The compressive strength of concrete, the yield strength of steel, the diameter of reinforcement and the number of reinforcements have a certain impact on the bearing capacity of the specimen. The ultimate bending moment of the specimen increases significantly with the increase of steel ratio and steel yield strength.

(5) The calculation formula of flexural capacity of reinforced hollow concrete filled square steel tubular member was proposed, and the accuracy of the calculation value of the formula is verified by the experimental data.

Acknowledgements

The research was supported by National Natural Science Foundation of China (52178148, 51808353), Excellent Youth Fund of Liaoning Province (2021-YQ-10), Xingliao Talent Program of Liaoning Province (XLYC2203109), Fundamental scientific research project of Liaoning Provincial Department of Education (LJKZ0598).

References

[1] Han L. H., Li W. and Bjorhovde R., “Developments and advanced applications of concrete-filled steel tubular (CFST) structures: Members”, Journal of Constructional Steel Research, 100, 211-228, 2014,

[2] Han, L.H., Li W., Wang W.D. and Tao, Z., Advanced composite and mixed structures: testing, theory and design approach (Second Edition), Science Press, Beijing, 2017.

[3] Kang J.Y., Choi E.S., Chin W.J. and Lee J.W., “Flexural behavior of concrete-filled steel tube members and its application”, International Journal of Steel Structures, 7, 319–324, 2007.

[4] Li G.C., Liu D., Yang Z.J. and Zhang, C.Y., “Flexural behavior of high strength concrete filled high strength square steel tube”, Journal of Constructional Steel Research, 128(1), 732-

744, 2017.
[5] Elchalakani M., Zhao X.L. and Grzebieta R.H., "Concrete-filled circular steel tubes subjected to pure bending", Journal of Constructional Steel Research, 57, 1141-1168, 2001.
[6] Han L.H., "Flexural behaviour of concrete-filled steel tubes", Journal of Constructional Steel Research, 60, 313-337, 2004,
[7] Han L. H., Lu H., Yao G.H. and Liao F.Y., "Further study on the flexural behaviour of concrete-filled steel tubes", Journal of Constructional Steel Research, 62, 554-565, 2006.
[8] Elchalakani M. and Zhao X. L., "Concrete-filled cold-formed circular steel tubes subjected to variable amplitude cyclic pure bending", Engineering Structures, 30, 287-299, 2008,
[9] Moon J., Roeder C.W. and Lee H.H., "Analytical modeling of bending of circular concrete-filled steel tubes", Engineering Structures, 42, 349-361, 2012.
[10] Wang R., Han L.H., Nie J.G. and Zhao X.L., "Flexural performance of rectangular CFST members", Thin-Walled Structures, 79, 154-165, 2014.
[11] Zhan Y.L., Zhao R.D., Ma John Z.G., Xu, T.F. and Song R.N., "Behavior of prestressed concrete-filled steel tube (CFST) beam", Engineering Structures, 122, 144-155, 2016.
[12] Javed, M.F., Sulong N.H.R., Memon S.A., Rehman S.K.Ur. and Khan N.B., "FE modelling of the flexural behaviour of square and rectangular steel tubes filled with normal and high strength concrete", Thin-Walled Structures, 119, 470-481. 2017.
[13] Chen Y., Feng R. and Gong W.Z, "Flexural behavior of concrete-filled aluminum alloy circular hollow section tubes", Construction and Building Materials, 165, 173-186, 2018.
[14] Al-shaar A.A.M. and Göğüş M.T., "Flexural behavior of lightweight concrete and self-compacting concrete-filled steel tube beams", Journal of Constructional Steel Research, 149, 153-164, 2018.
[15] Liu, D., Zuo J., Wang, J., Duan, K., Zhang, D.M. and Guo, S., "Bending failure mechanism and strengthening of concrete-filled steel tubular support", Engineering Structures, 2019, 198: 109449.
[16] Al Zand A.W. and Badaruzzaman W.H.W., "Flexural performance of square concrete-filled steel tube beams stiffened with V-shaped grooves", Journal of Constructional Steel Research, 166, 105930, 2020.
[17] Li G.C., Qiu Z.M., Yang Z.J., Chen B.W. and Feng Y.H., "Seismic performance of high strength concrete filled high strength square steel tubes under cyclic pure bending", Advanced Steel Construction, 16, 112-123, 2020.
[18] Li, J.Y., Deng, Z.C. and Sun, T., "Flexural behavior of ultra-high performance concrete filled high-strength steel tube", Structural Concrete, 22, 1688-1707, 2021.
[19] Wang Y., Lin, H., Lai Z.C., Li D., Zhou W,S. and Yang X.Q., "Flexural behavior of high-strength rectangular concrete-filled steel tube members", Journal of Structural Engineering, 148, 04021230, 2022.
[20] Kodur V.K.R. and MacKinnon D.H., "Simplified design of concrete-filled hollow structural steel columns for fire endurance", Journal of Constructional Steel Research, 46, 298, 1998.
[21] Song Y.L. and Chen J. F., "Structural behaviour of short steel—concrete composite spun tubular columns", Magazine of Concrete Research, 52, 411-418, 2000.
[22] Kvedaras A.K. and Kudzys A., "The structural safety of hollow concrete-filled circular steel members", 2006, 62(11), 1116-1122, Journal of Constructional Steel Research.
[23] Chen J., Jin W.L., Fu J., "Experimental investigation of thin-walled centrifugal concrete-filled steel tubes under torsion", Thin-Walled Structures, 46, 1087-1093, 2008,
[24] Zhao Y.G., Yan X.F. and Lin S.Q., "Compressive strength of axially loaded circular hollow centrifugal concrete-filled steel tubular short columns", Engineering Structures, 201, 109828, 2019.
[25] Yang Z.J., Han J.M., Lei Y.Q., Li G.C. and Liu S.Q., "A reinforced high-strength concrete-filled hollow steel tubes column", Chinese Patent, ZL 201821067732. 2, 2019.
[26] Guo, Z.H., "Strength and constitutive relationship of concrete - principle and application", China Construction Industry Press, Beijing, 1994.
[27] Han L.H., Yao G.H. and Tao, Z., "Performance of concrete-filled thin-walled steel tubes under pure torsion", Thin-Walled Structures, 45, 24-36, 2007.
[28] Han L.H.," Concrete filled tubular structure: theory and practice", Science Press, Beijing, 2016.
[29] Zhang S., "Mechanical behavior of reinforced hollow high strength concrete filled square steel tube members under pure bending", Shenyang Jianzhu University, MS Thesis, 2023.